Int J Thermophys (2008) 29:1606–1614
DOI 10.1007/s10765-007-0342-4

Performance and Validation Tests on the NIST Hybrid Humidity Generator

C. W. Meyer · W. W. Miller · D. C. Ripple · G. E. Scace

Published online: 30 January 2008

Abstract A new humidity generator has been constructed at the National Institute of Standards and Technology. Once fully operational, the NIST hybrid humidity generator (HHG) will generate frost/dew points from −70°C to +85°C using calibration gas-flow rates up to 150 standard liters per minute and is expected to outperform the present humidity generator at NIST in terms of accuracy. The HHG combines the two-pressure and divided-flow humidity-generation techniques (hence, the name "hybrid"). The centerpiece of the HHG is a heat exchanger/saturator that is immersed in a temperature-controlled bath stable to within 1 mK. For dew/frost-point temperatures above −15°C, the two-pressure principle is employed. For frost points at or below −15°C, the water-vapor/air mixture is produced by mixing metered streams of moist air produced by the two-pressure method with purified, dry air. A series of performance and validation tests on the HHG in the two-pressure mode, including measurements of temperature gradients and pressure stability in the generator under various operating conditions, and comparison of the humidity generated by the HHG to that generated by the other NIST humidity-generation standards, are reported.

Keywords Calibration · Generator · Humidity · Hygrometer · Saturator · Standards · Water vapor

1 Introduction

The National Institute of Standards and Technology (NIST) has constructed a new primary standard humidity generator [1]. The facility is called the hybrid humidity

C. W. Meyer (✉) · W. W. Miller · D. C. Ripple · G. E. Scace
Process Measurements Division, National Institute of Standards and Technology, Gaithersburg, MD 20899, USA
e-mail: cmeyer@nist.gov

generator (HHG) and is so named because it incorporates the two-pressure and divided-flow humidity-generation principles [2] into a single design. Once commissioned, it will replace the NIST Two-Pressure Humidity Generator Mark 2 [3,4] (known as the "2-P" generator) as the principal standard humidity generator for calibration of customer hygrometers. The NIST low frost-point generator (LFPG) [5] will remain in operation as a complement to the HHG, being used primarily at frost-point temperatures below −70°C. The HHG is designed to accommodate gas flows up to $150\,\mathrm{l}\cdot\mathrm{min}^{-1}$. The lower frost-point limit of the HHG is −70°C, which is that of the 2-P generator. The higher dew-point limit of the HHG is 85°C, which at ambient pressure corresponds to a water-vapor mole fraction of approximately 57%. This limit is considerably higher than the 22°C dew-point limit (2.6% water-vapor mole fraction) of the 2-P generator. The increase in dew-point limit enables NIST to address the need of the semiconductor and fuel-cell industries for high-range humidity standards. In addition, the humidity generated by the HHG has lower uncertainty than that from the 2-P generator. Finally, the HHG is easier, safer, and less expensive to operate than the 2-P generator.

In this article, we discuss recent measurements to test the performance of the HHG while in the two-pressure mode. These measurements include determinations of temperature stability and gradients in the bath surrounding the HHG's final saturator and pressure stability and temperature gradients inside the saturator. From these measurements, we find that the HHG operating in the two-pressure mode has an expanded dew-point uncertainty ($k = 2$) that is dependent on temperature and pressure and varies from 10 to 30 mK.

2 Generator Design

2.1 Saturation System

The design of the saturation system is described in full detail elsewhere [1]. Briefly, the saturation system of the HHG consists of a pre-saturator and final saturator. The pre-saturator accomplishes virtually all of the saturation; the final saturator performs small adjustments to ensure that the generated humidity is constant and determinable with minimal uncertainty.

The final saturator is composed of a heat exchanger located immediately above a saturation chamber. Both systems rest inside a commercially made temperature-controlled bath with a volume of 167 l that is uniform to within 2 mK at 25°C. The heat exchanger brings the temperature of the incoming gas to within 1 mK of the saturation chamber temperature; by doing so, the exchanger minimizes latent heat loading on the chamber from the gas as it enters. In addition, the heat exchanger condenses out any moisture above the dew point of the saturation chamber; this condensed water drains into the saturation chamber. The stainless-steel heat exchanger consists of two header tanks separated by an array of 116 parallel tubes with an inner diameter of 7.8 mm and a length of 48.5 cm. With these dimensions and with a gas flow of $150\,\mathrm{l}\cdot\mathrm{min}^{-1}$, the gas will flow through the parallel tubes for a period of about ten thermal time constants. The stainless-steel saturation chamber contains a 2.2 cm layer of water and a 2.2 cm layer of gas above it, covering a horizontal area of $0.28\,\mathrm{m}^2$. Dividers inside the

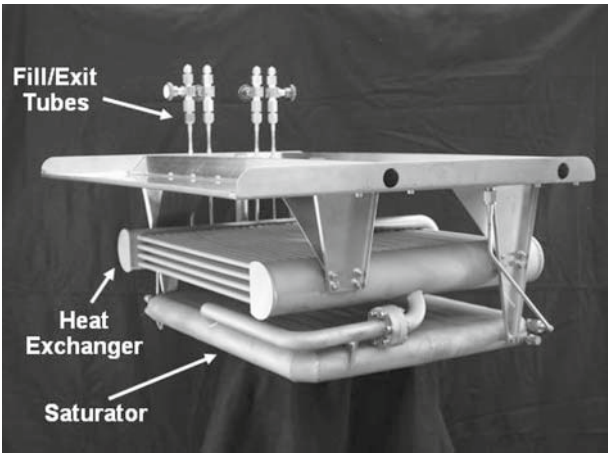

Fig. 1 Photograph of the HHG final saturator, including the heat exchanger and the saturation chamber

saturator partition the chamber into two, equal-area channels that follow a serpentine path. Twisted vanes welded to the dividers improve mixing between the gas and water vapor while the gas is in the saturation chamber.

The mole fraction x of water vapor in the gas is then calculated using the equation,

$$x = \frac{e_{\mathrm{w}}(T_{\mathrm{s}})}{P_{\mathrm{s}}} f(T_{\mathrm{s}}, P_{\mathrm{s}}) \tag{1}$$

where T_{s} and P_{s} are the temperature and pressure of the gas and water in the saturator, and $e_{\mathrm{w}}(T_{\mathrm{s}})$ is the water-vapor pressure at T_{s} as calculated by [6,7]. The enhancement factor $f(T_{\mathrm{s}}, P_{\mathrm{s}})$, described and calculated in [8], reflects departures from ideal solution behavior and non-ideal gas effects.

We measure the temperature of the saturator using a standard platinum resistance thermometer (SPRT) immersed in the temperature-controlled bath in conjunction with an AC resistance bridge. A silicon strain gauge connected to a point in the saturator near the gas outlet using stainless-steel tubing measures the saturator pressure. Pressure measurements downstream of the saturation chamber (for dew-point determination) are made with a quartz-crystal-resonator pressure transducer. The bridge and both pressure gauges are interfaced to a computer.

Figure 1 shows the entire heat-exchanger/final-saturator system. The system is suspended from a horizontal plate that also serves as the top cover to the bath. Two sets of water fill tubes and gas outlet tubes can be seen in the figure, one for each channel.

2.2 Two-Pressure and Divided-Flow Methods

The two-pressure technique [2] involves saturating the gas at an elevated pressure and afterward expanding the gas down to ambient pressure. In the HHG, the saturator may be pressurized up to 550 kPa; the gas then passes through an expansion valve

that controls the saturator pressure by adjusting the gas-flow rate out of the saturator. The valve is located outside the temperature-controlled bath, downstream from the saturation chamber. The expansion valve is a butterfly-vane valve with a high-speed motor/gear assembly, adjusted by a PID controller that senses the pressure using the strain gauge mentioned above.

The divided-flow method [2] involves diluting the saturated gas with dry gas using precisely metered streams of gas. Such a technique allows generation of arbitrarily low-humidity values while operating the saturator at convenient temperatures. The design of the divided-flow system for the HHG is described in [1]. When performing hygrometer calibrations, the HHG will use the divided-flow method for mole fractions less than 1.2×10^{-3} (frost points less than $-18°C$).

3 Performance and Validation Tests

Performance tests were made on the HHG in the two-pressure mode to determine components of an uncertainty budget for the generator. Specifically, measurements were made of temperature gradients and temperature stability in the saturator bath, and temperature gradients and pressure stability inside the saturation chamber.

Temperature non-uniformities in the bath were measured employing five type K thermocouples used in differential mode, measured with an 8½ digit multimeter through a scanner with low thermal emfs. For these measurements, there was no gas flow through the saturator. We attached the reference junction of each thermocouple to the exit point from the saturator chamber and placed the measuring junction in thermal contact with the location of interest. The locations examined were the entrance to the heat exchanger, the exit from the heat exchanger, the entrance to the saturation chamber, the bath below the saturation chamber, and the bath above the saturation chamber. Figure 2 shows the temperature non-uniformities measured. Between 0°C and 40°C, the non-uniformities are within the resolution of the measurements. At 60°C non-uniformities become observable, and at 85°C they reach 16 mK. However, the largest gradients are vertical, with the top of the bath being cooler than the bottom. These non-uniformities may be reduced in the future once improved methods to insulate the top of the bath (e.g., flotation balls) are employed.

We also measured the thermal effects of pre-saturated gas flowing through the saturator. The measurements were made using two metal-sheathed, type T thermocouples that are mounted with measuring junctions near the saturator entrance. The junction of the first thermocouple is immersed in the water and that of the second is located in the gas stream. Figure 3 shows the temperature difference between the thermocouple junction when gas flows through the generator and when no gas flows through it (assumed to be the bath temperature). For this plot, the bath temperature is 22°C, the gas flow is $50 l \cdot min^{-1}$, and the differences are plotted as a function of the pre-saturator dew point. When the pre-saturator dew point is considerably less than the bath temperature, temperature non-uniformities occur due to evaporative cooling of the water in the chamber. When the dew point is 8°C below the bath temperature, the non-uniformity is larger than 0.1°C. However, no non-uniformities are resolvable when the dew point is above the bath temperature; in this case, the excess moisture condenses in the heat

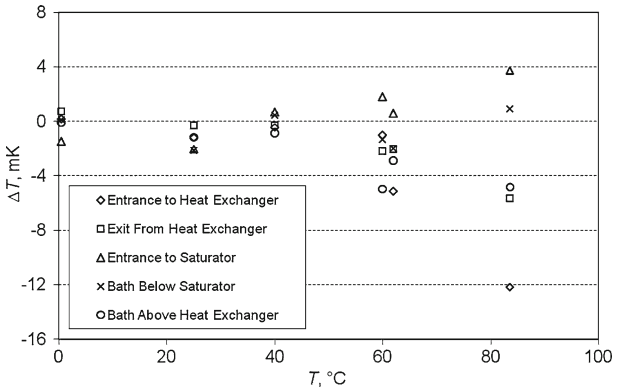

Fig. 2 Temperature non-uniformities in the bath containing the final saturator, as measured by differential type K thermocouples attached to the outside of the saturator. The plot displays temperature differences between the designated location and the exit point from the saturation chamber

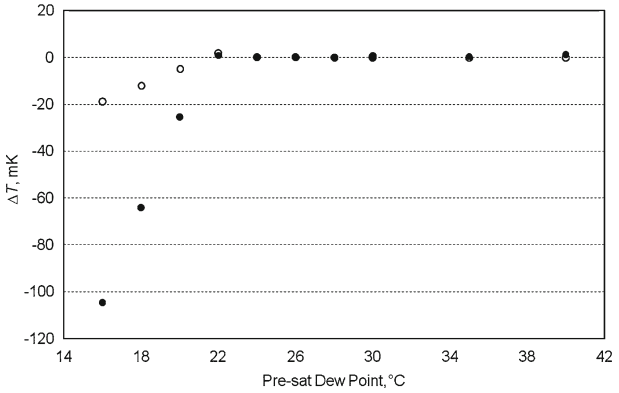

Fig. 3 Temperature deviations from the bath temperature inside the saturation chamber at the entrance to the chamber when gas is flowing through it. The flow rate is $50\,l \cdot \mathrm{min}^{-1}$, and the bath temperature is 22°C. The deviations are plotted as a function of the pre-saturator dew point. The solid and open circles are from type T thermocouples (used in absolute mode) placed in the water and gas, respectively. Here, $\Delta T = T_{\mathrm{flow}} - T_{\mathrm{no\ flow}}$, where T_{flow} and $T_{\mathrm{no\ flow}}$ are the measured temperatures with and without gas flow, respectively. $T_{\mathrm{no\ flow}}$ is assumed to be the bath temperature

exchanger and is at thermal equilibrium with the saturation chamber by the time it enters the chamber. These measurements demonstrate the importance of setting the pre-saturator to a dew point above, rather than below, the bath temperature.

In addition, we measured the stability of the bath over 1200 s at a series of bath temperatures. The results are shown in Fig. 4. At 20°C, the standard deviation was at a minimum, at 0.2 mK. As the bath temperature was lowered, the standard deviation reached 0.9 mK at 0.5°C and as it was raised, the standard deviation reached 1.1 mK at 85°C.

By monitoring pressure fluctuations in the saturation chamber, we first optimized the PID settings of the pressure controller and then measured the pressure variations at the optimum settings. At a saturator temperature of 20°C with a variety of pressures

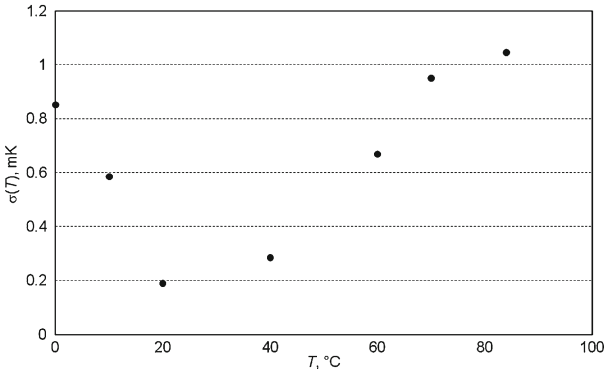

Fig. 4 Standard deviation of the temperature fluctuations in the bath containing the final saturator as a function of bath temperature, as measured by an SPRT

and flow rates up to $150\,\mathrm{l}\cdot\mathrm{min}^{-1}$, the standard deviation was less than 15 Pa. However, since pressure is controlled by adjustments of the gas flow rate out of the saturation chamber, optimal pressure control results in noticeable gas-flow fluctuations. Therefore, less-than-optimal PID settings may be required to keep gas-flow fluctuations at acceptable levels.

Self-consistency tests were conducted by using a chilled-mirror hygrometer as a transfer standard. We performed a four-wire resistance measurement of the hygrometer's platinum resistance thermometer (PRT), which is in thermal contact with its mirror. The hygrometer dew-point temperature, as determined by the PRT, was then calculated with the Callendar-van Dusen equation [9], using 100 Ω as the assumed PRT resistance at 0°C. For the self-consistency tests, dew-point temperatures T_{DP} were generated with eight different saturator temperatures and saturator pressures ranging from 500 kPa to ambient. The flow rate through the generator was $30\,\mathrm{l}\cdot\mathrm{min}^{-1}$, and $0.5\,\mathrm{l}\cdot\mathrm{min}^{-1}$ of this flow was directed through the hygrometer. The difference between the hygrometer-measured T_{DP} and the generated T_{DP}, ΔT_{DP}, was then plotted for each dew point of the set. Figure 5 shows ΔT_{DP} as a function of T_{DP}. When the saturator temperature was at 30°C and above, the seven saturator pressures used were approximately 100, 125, 150, 200, 300, 400, and 500 kPa. For $T_{\mathrm{s}} = 20°\mathrm{C}$, this pressure combination was used with the exception of the 200 kPa point, and for $T_{\mathrm{s}} = 10°\mathrm{C}$, the combination was used with additional points at 175, 250, and 350 kPa. For a given T_{s}, the dew point decreases monotonically with increasing saturator pressure. The agreement between similar dew-point temperatures that are generated at different saturator temperatures, indicated with different symbols, provides information on the degree of self-consistency of the HHG. The standard deviation of the values of ΔT_{DP} from their mean value is 6 mK. This is approximately the size of the standard uncertainty of the hygrometer measurement due to reproducibility, which we estimate to be 5 mK.

4 Uncertainty Budget

Based on these performance tests, as well as measurement equipment specifications, we have constructed a preliminary uncertainty budget for the HHG while using the

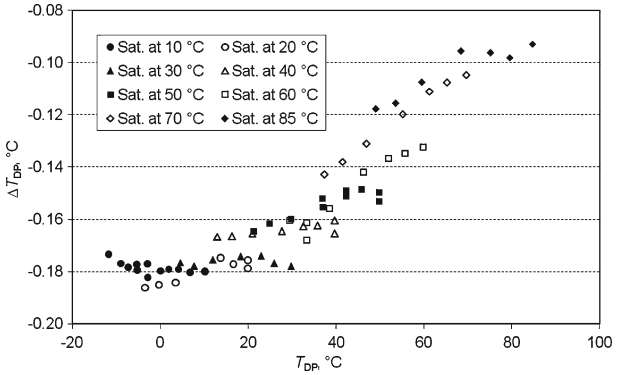

Fig. 5 Comparison of dew-point temperatures T_{DP} generated by the HHG using different combinations of the saturator temperature T_s and pressure P_s. The comparisons were made using an uncalibrated chilled-mirror hygrometer as a transfer standard. Here, ΔT_{DP} is the measured T_{DP} minus the generated T_{DP}. Measurements with the saturator at different temperatures are plotted with different symbols

two-pressure method; the budget is shown in Table 1. The budget is still preliminary because we intend to make additional performance tests that may change our uncertainty assessments, such as measuring bath-temperature non-uniformities under conditions of gas flow. In the budget, the uncertainty for the calculation of $e_w(T_s)$ is obtained from Table 2 of [10]. The uncertainty for the calculation of $f(T_s, P_s)$ is presented as a fit to the data of Table 9 in [11]; here, the "maximum percentage uncertainties" from the table were divided by $\sqrt{3}$ to obtain the standard uncertainty. The uncertainty for the calculation of $f(T_s, P_s)$, $u(f)$, is quite large for some operating conditions, while the uncertainty of $e_w(T_s)$ is negligible. At $P_s = 100$ kPa, where $u(f)$ gives no contribution to the dew-point total expanded uncertainty U_{tot}, the value of $U_{tot}(k = 2)$ is 8 mK for $T_s < 40$°C and is dominated by the uncertainty for pressure measurement and stability. For $T_s \geq 40$°C, temperature non-uniformities in the bath become influential, and U_{tot} reaches 20 mK at $T_s = 85$°C. Consider next the opposite extreme of operating pressure, $P_s = 500$ kPa. At $T_s = 0.5$°C, where $u(f) = 0.08\%$, $U_{tot} = 24$ mK and it is dominated by $u(f)$. As T_s is increased, $u(f)$ and U_{tot} decrease until $U_{tot} = 17$ mK at $T_s = 70$°C. Above this temperature, U_{tot} increases by 0.4 mK until $T_s = 85$°C as bath temperature non-uniformities again become the dominant uncertainty. Accounting for the expanded uncertainty of the hygrometer reproducibility, the results of the self-consistency tests described above are compatible with the estimated uncertainties of the generator.

5 Comparisons with Other NIST Generators

Finally, comparison measurements were made with the two other generators used at NIST, the 2-P generator and the LFPG, using the chilled-mirror hygrometer as a transfer standard. Figure 6 shows values of ΔT_{DP} for the three generators over the range from −15°C to 30°C. The data from the HHG are those shown in Fig. 5. For measurements below 0°C, the gas moisture was observed to condense on the mirror

Table 1 Uncertainty budget for the hybrid humidity generator in two-pressure mode

Uncertainty element	Standard uncertainty	Uncertainty unit
Temperature measurement	0.25	mK
Temperature non-uniformities in bath	1, ($T \leq 40°C$)	
	$0.16T/°C - 5.4$, ($T > 40°C$)	mK
Temperature stability	1	mK
Saturator pressure measurement	15	Pa
Saturator pressure stability	20	Pa
Downstream pressure measurement	15	Pa
Calculation of $e_w(T_s)$	44	$Pa \cdot MPa^{-1}$
Calculation of $f(T_s, P_s)$	$P_s/(10^7 \cdot Pa) \cdot (18.3\,K/T_s - 0.047)$	–
Total dew-point temperature	$3 \leq u_{tot} \leq 12$	mK

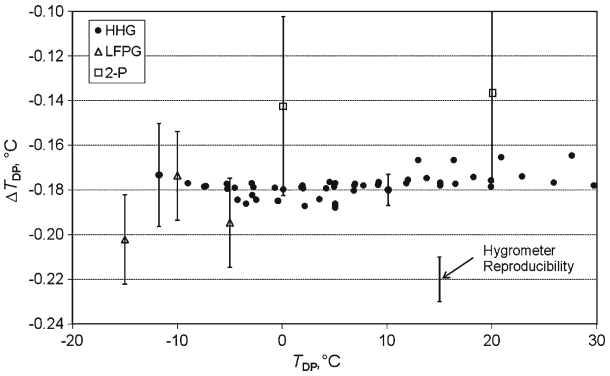

Fig. 6 Comparison of dew points generated by the HHG with those generated by the NIST two-pressure (2-P) generator and the NIST low frost-point generator. The comparisons were made by making ΔT_{DP} measurements using a chilled-mirror hygrometer as a transfer standard. The combined expanded uncertainties of the LFPG and 2-P generator are shown as error bars. The combined expanded uncertainty of the HHG is shown for two points with $T_s = 10°C$, one where the uncertainty is minimal ($P_s = 100\,kPa$, $T_{DP} = 10°C$) and one where it is at a maximum ($P_s = 500\,kPa$, $T_{DP} = -12°C$). The uncertainty due to hygrometer reproducibility is also shown

as dew rather than frost. Error bars show the total expanded ($k = 2$) uncertainty for T_{DP} from the generators. The expanded uncertainty due to the hygrometer reproducibility is also shown. For the dew-point temperatures generated, these uncertainties for the 2-P generator and LFPG are 40 mK [4] and 20 mK [12], respectively. The HHG and LFPG agree within 10 mK, which is within the combined expanded uncertainties of the two generators and the hygrometer reproducibility. The HHG and 2-P generator agree within 40 mK; the difference is also within the combined expanded uncertainties, although the agreement is not as good as that between the HHG and LFPG.

Acknowledgments The authors gratefully thank Joseph T. Hodges and David Allen for useful discussions.

References

1. G.E. Scace, C.W. Meyer, W.W. Miller, J.T. Hodges, in *Proceedings of the 5th International Symposium on Humidity and Moisture* (in press)
2. A. Wexler, Tappi **44**, 180A (1961)
3. S. Hasegawa, J.W. Little, J. Res. Natl. Bur. Stand. (U.S.) **81A**, 81 (1977)
4. P.H. Huang, in *Papers and Abstracts from the Third International Symposium on Humidity and Moisture* (National Physical Laboratory, Teddington, UK, 1998), pp. 149–158
5. G.E. Scace, D.C. Hovde, J.T. Hodges, P.H. Huang, J.A. Silver, J.R. Whetstone, in *Papers and Abstracts from the Third International Symposium on Humidity and Moisture* (National Physical Laboratory, Teddington, UK, 1998), pp. 180–190
6. A. Saul, W. Wagner, J. Phys. Chem. Ref. Data **16**, 893 (1987)
7. W. Wagner, A. Pruss, J. Phys. Chem. Ref. Data **22**, 783 (1993)
8. R.W. Hyland, A. Wexler, ASHRAE Trans. **89-IIa**, 520 (1983)
9. ASTM Standard E 1137/E 1137M-04, *Annual Book of ASTM Standards*, vol. 14.03 (ASTM International, Conshohocken, PA, 2006), pp. 473–479
10. A. Wexler, J. Res. Natl. Bur. Stand. (U.S.) **80A**, 775 (1976)
11. R.W. Hyland, J. Res. Natl. Bur. Stand. (U.S.) **79A**, 551 (1975)
12. G.E. Scace, J.T. Hodges, in *Proceedings of TEMPMEKO 2001, 8th International Symposium on Temperature and Thermal Measurements in Industry and Science*, ed. by B. Fellmuth, J. Seidel, G. Scholz (VDE Verlag, Berlin, 2002), pp. 597–602